FULL ARTICLE

Polarized light microscopy for 3-dimensional mapping of collagen fiber architecture in ocular tissues

Bin Yang[1] | Ning-Jiun Jan[1,2] | Bryn Brazile[1] | Andrew Voorhees[1] | Kira L. Lathrop[1,2] | Ian A Sigal[1,2]* (ORCID)

[1]Department of Ophthalmology, University of Pittsburgh School of Medicine, Pittsburgh, Pennsylvania

[2]Department of Bioengineering, University of Pittsburgh, Pittsburgh, Pennsylvania

*Correspondence
Ian A. Sigal, Ocular Biomechanics Laboratory, Department of Ophthalmology, University of Pittsburgh School of Medicine, 203 Lothrop Street, Rm 930, Pittsburgh, PA 15213.
Email: ian@ocularbiomechanics.com

Funding information
Eye and Ear Foundation (Pittsburgh), Grant/Award Number: NA; National Institutes of Health, Grant/Award Numbers: R01-EY023966, R01-EY025011, T32-EY017271, P30-EY008098; Research to Prevent Blindness (NY), Grant/Award Number: Award to the Dept. of Ophthalmology, UPMC

Collagen fibers play a central role in normal eye mechanics and pathology. In ocular tissues, collagen fibers exhibit a complex 3-dimensional (3D) fiber orientation, with both in-plane (IP) and out-of-plane (OP) orientations. Imaging techniques traditionally applied to the study of ocular tissues only quantify IP fiber orientation, providing little information on OP fiber orientation. Accurate description of the complex 3D fiber microstructures of the eye requires quantifying full 3D fiber orientation. Herein, we present 3dPLM, a technique based on polarized light microscopy developed to quantify both IP and OP collagen fiber orientations of ocular tissues. The performance of 3dPLM was examined by simulation and experimental verification and validation. The experiments demonstrated an excellent agreement between extracted and true 3D fiber orientation. Both IP and OP fiber orientations can be extracted from the sclera and the cornea, providing previously unavailable quantitative 3D measures and insight into the tissue microarchitecture. Together, the results demonstrate that 3dPLM is a powerful imaging technique for the analysis of ocular tissues.
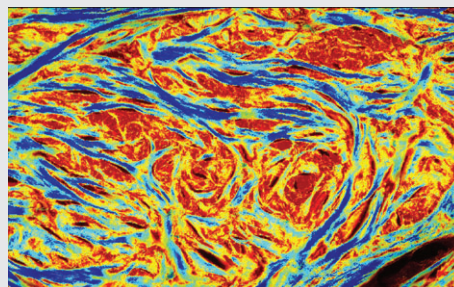
KEYWORDS

collagen, eye, orientation, polarized light microscopy, sclera

1 | INTRODUCTION

The collagen fibers of the eye have a complex 3-dimensional (3D) organization that is central to the normal functioning of the eye. For example, a distinct organization is necessary for cornea shape and transparency [1–3], and for structural support of the posterior sclera [4, 5]. Fiber organization is also believed to play an important role in several ocular pathologies, such as myopia, glaucoma and keratoconus [6–9]. Studying the eye's collagen fiber microstructure is therefore fundamental to understanding its roles in both health and disease.

Several imaging techniques have been developed and used to quantify fiber orientations in ocular tissues, including small angle light scattering (SALS) [10], wide-angle X-ray scattering (WAXS) [7, 11] and polarized light microscopy (PLM) [12–14]. These imaging techniques, while very helpful, have an important limitation: they provide very limited information, if any, of the full 3D orientation of the collagen fibers. Multiphoton microscopy, including second harmonic generation (SHG) imaging, can reveal tissue microstructures with high resolution and specificity [15, 16]. Although many studies using SHG for fiber orientation focus 2-dimensional (2D) measures, there

are 3D models [17]. The fibers are oriented in 3D, with both in-plane (IP) and out-of-plane (OP) fiber orientation components. The IP fiber orientation is the projected fiber orientation in the observation plane, while the OP fiber orientation measures the angle between the fiber and observation plane. The techniques described above, typically only quantify IP fiber orientation and the equally important OP fiber orientation is not quantified.

In this work, we demonstrate that studying 3D fiber structures with 2D information is not only insufficient but can also potentially lead to inaccurate interpretations and incorrect conclusions. We present 3dPLM as an imaging technique that allows quantifying collagen fiber orientation in 3D in ocular tissues. 3dPLM is an extension of PLM, which we recently demonstrated as a robust and effective approach for mapping IP fiber orientation in ocular tissues [12].

2 | MATERIALS AND METHODS

We will first describe the theoretical background of 3D fiber orientation quantification with 3dPLM. Next, we will examine its robustness and performance using both simulation and experimental analysis of tissue samples with known fiber orientations. Finally, we will apply 3dPLM to quantify and visualize 3D fiber orientation in various regions of ocular tissues.

2.1 | Theoretical background

The birefringent property of collagen fibers has been well studied. In collagen fibers, the slow axis is along fibers and the fast axis is perpendicular to fibers. The light propagation in collagen fibers can be studied using the theory previously described by Born and Wolf [18], which is briefly described below. The light propagating velocity ν with unit wave vector $\vec{s}$ in collagen fibers can be described using the Fresnel equation:

$$\frac{s_x^2}{v^2 - v_x^2} + \frac{s_y^2}{v^2 - v_y^2} + \frac{s_z^2}{v^2 - v_z^2} = 0. \quad (1)$$

The unit wave vector can be decomposed in the spherical coordinates system as:

$$\vec{s} = \begin{pmatrix} s_x \\ s_y \\ s_z \end{pmatrix} = \begin{pmatrix} \sin\theta\cos\varphi \\ \sin\theta\sin\varphi \\ \cos\theta \end{pmatrix}. \quad (2)$$

The ν_x, ν_y and ν_z are the principal velocities along the orthogonal x-, y- and z-axis, respectively. The velocity can be expressed as a function of the dielectric constant ε:

$$v = c/\sqrt{\varepsilon}. \quad (3)$$

In collagen fibers, dielectric constant $\varepsilon_x = \varepsilon_y = n_o^2$ and $\varepsilon_z = n_e^2$, where n_o and n_e are the refractive index of ordinary wave and extraordinary wave, respectively. The n_e is the refractive index along the fibers while n_o is the refractive index perpendicular to the fibers. With this relationship and Eqs. (2) and (3), Eq. (1) can be simplified as:

$$(n^2 - n_0^2)\left[n_0^2\left(s_x^2 + s_y^2\right)(n^2 - n_e^2) + s_z^2 n_e^2 (n^2 - n_0^2)\right] = 0. \quad (4)$$

By solving Eq. (4), we obtained:

$$n_1 = n_o, \quad (5)$$

and

$$n_2 = \frac{n_o n_e}{\sqrt{n_0^2 \sin^2\theta + n_e^2 \cos^2\theta}}. \quad (6)$$

Thus, the effective birefringence along the light propagation direction in collagenous tissues can be expressed as:

$$\Delta n = n_2 - n_1 = \frac{n_o n_e}{\sqrt{n_0^2 \sin^2\theta + n_e^2 \cos^2\theta}} - n_o. \quad (7)$$

For a small refractive index n, Eq. (7) can be approximated as [19]:

$$\Delta n \approx (n_e - n_o)\sin^2\theta \text{ or } \Delta n \approx (n_e - n_o)\cos^2\phi, \quad (8)$$

where φ is the OP angle and thus the phase retardance introduced by collagenous tissue with a thickness of d is:

$$\delta(\phi) = \frac{2\pi(n_e - n_o)d}{\lambda} \cdot \cos^2\phi. \quad (9)$$

Equation (9) shows that effective retardance is dependent on the OP angle of fibers. Given the thickness, the light accumulates maximal retardance when all fibers are IP and zero retardance when they are OP by 90°. Equation (9) can be further simplified as $\delta(\phi) = \delta_0 \cdot \cos^2\phi$, where $\delta_0 = \frac{2\pi(n_e - n_o)d}{\lambda}$. The δ_0 represents the retardance from fibers that are perfectly IP and δ_0 can be experimentally obtained from apparent IP fibers of the sample.

Various PLM techniques have been developed to quantify tissue retardance experimentally. Here, we used the same approach as in our previous IP fiber orientation mapping study [12]. Four intensity measurements I_0, I_{45}, I_{90} and I_{135}, are taken with linear polarizer set to 0°, 45°, 90° and 135°, respectively. Then the retardance can be calculated as:

$$\delta = \sin^{-1}\left(\frac{2\sqrt{(I_{90} - I_0)^2 + (I_{135} - I_{45})^2}}{I_0 + I_{45} + I_{90} + I_{135}}\right). \quad (10)$$

The OP fiber orientation φ can be calculated by combining Eqs. (9) and (10). The IP fiber orientation is calculated as previously reported [12]. Briefly, local fiber orientation is computed at each pixel. For visualization, the collagen fiber orientation map is weighted by an "energy" map, where energy is calculated as:

$$energy^2 = (I_{90} - I_0)^2 - (I_{135} - I_{45})^2. \qquad (11)$$

With this definition, the energy value is high when there is a substantial change in signal with angle, and low with small changes.

2.2 | Simulation of the effects of birefringence and retardance approximation

We used the approximate form of birefringence shown in Eq. (8) to describe collagen fiber birefringent properties. To examine how this approximation affects the OP angle quantification, we calculated and compared Δn over OP angles between 0° and 90° using both exact and approximate forms. The parameters used in the calculation were chosen to reflect conditions of the later experiments. The n_o at 535 nm of collagen fibers was calculated as 1.480 using the refractive index dispersion formula of collagen fibers previously described [20]. The n_e was calculated as 1.483 based on birefringence $\Delta n = 0.003$, which has been well studied and documented [21].

If the retardance of IP fibers is not known, it must be estimated, which may introduce approximation error in the quantification of IP fiber orientation. We performed a numerical simulation to study how robust our method is if such error is present. In the simulation, we first calculated true retardance δ_0 based on representative tissue parameters. Then, we randomly generated 200 retardance values, δ_0', uniformly distributed within $+/-10\%$ of the true retardance δ_0 to represent approximation error. We selected 10% as large enough to account for approximation errors in ocular tissues based on preliminary work not shown here. OP angle-dependent retardance δ was then calculated with OP angle varying from 0° to 90° every 15°. The OP angle was then computed using Eq. (11) by replacing δ_0 with one of 200 δ_0' values and this quantification process was repeated 200 times. The mean and SD of calculated OP angle values

were computed. During the analysis, if the measured retardance is larger than estimated retardance δ_0', the calculated OP angle was then set to zero.

2.3 | 3dPLM imaging system

A commercial microscope system (Olympus, IX83, Tokyo, Japan) was customized to achieve automated polarized light imaging. A circular polarizer with a wavelength range of 400 to 700 nm (Edmund Optics, #88-099, Barrington, New Jersey) and an interference band-pass filter centered at 535 nm with a passband of 64.4 nm (Olympus, IF550, Tokyo, Japan) were placed in the illumination path to achieve circularly polarized light illumination. In the image acquisition path, 4 linear polarizers (Chroma, 21003b) were placed into a motorized filter wheel (Prior Scientific Inc., HF108SIX3, Rockland, Massachusetts) to perform serial image acquisition at 4 polarization angles. The images were acquired with a 16bit CMOS camera (Hamamatsu, Flash 4.0 LT, Hamamatsu, Japan).

2.4 | Verification with chicken tendons

We verified the performance of this method by quantifying OP angles of cryosectioned chicken tendons. Chicken leg tendon was chosen for its simple and highly ordered collagen fiber organization [22], which is ideal for verification purposes. Chicken tendons were excised from fresh chicken legs purchased from a local grocery store. Collagen fibers run along the longitudinal direction of the tendon and they are naturally wavy. Such wavy features are recognized as collagen fiber crimp. To increase collagen fiber alignment and minimize fiber, the tendons were stretched with a uniaxial stretcher (S.T. JAPAN, STJ-0116mini, Tokyo, Japan). We made sure that tendons were well stretched by applying maximum stretch without breaking. While maintaining this stretch, the tendon was submerged in 10% formalin for fixation for about 12 hours. We have shown that formalin fixation causes only minimal changes in the overall shape or size of tissues [23], and in fiber retardance and orientation [12]. After fixation, the chicken tendons were cut into small rectangle pieces. Tendon pieces were later placed at 7 set OP angles and submerged in optimum cutting temperature (OCT) compound (Tissue-Plus, Fisher HealthCare, Houston, Texas) to be cryosectioned. The chicken tendon pieces were then sectioned at a thickness of 25 μm for 3dPLM imaging. A region within the sectioned tendon tissue was manually selected and the mean and SD of the estimated OP angles were calculated.

2.5 | 3dPLM imaging of ocular tissues

To demonstrate the applicability of 3dPLM over the corneoscleral shell and multiple species, we acquired images from human and sheep eyes spanning the anterior and posterior poles. The anatomy of the eye is shown in Figure 1 with major components and eye orientation illustrated. The sheep eye (<2 years old) was obtained from a local slaughterhouse
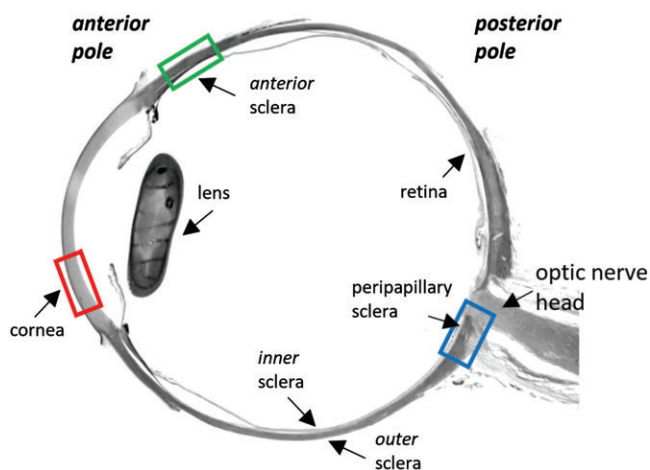

FIGURE 1   The anatomy of the eye with major components and orientation illustrated. The red, green and blue boxes indicate the locations of 3 regions selected for imaging

and underwent the same fixation and cryosectioning procedures described in Section 2.4 within 24 hours of death. The sheep eye was sectioned sagittally at 25 µm thickness, and sections were stored at 4°C until imaging. A section through the optic nerve head was selected. The tissue sections were rehydrated, cover slipped and kept hydrated while they were imaged with a ×4 strain free objective. In preliminary tests (results not shown), we confirmed that measurements obtained immediately after sectioning and months later are indistinguishable. The blue box in Figure 1 indicates the location of the imaged region. Sagittal sections of normal human eyes were prepared by the Department of Pathology at the University of Pittsburgh School of Medicine. Tissue preparation is critical for optical measurements, as has been thoroughly documented in studies of cornea [24–27]. The study was conducted in accordance with the tenets of the Declaration of Helsinki and the Health Insurance Portability and Accountability Act. Prior to obtaining the tissue, an independent party trained in HIPAA regulation verified that the samples had been appropriately deidentified. A 5 µm section of an ostensibly normal 27-year-old female was selected and 2 regions, cornea and anterior sclera, were imaged at ×40. The locations of imaged cornea and anterior sclera are indicated with red and green boxes, respectively. Both IP and OP fiber orientation maps, as well as a 3D fiber representation, were generated for all regions.

3 | RESULTS

3.1 | Simulation of the effects of birefringence and retardance approximation

Approximating birefringence and retardance had only a minimal impact on OP angle quantification. The birefringence calculated using exact and approximate forms are shown in Figure 2A. As the OP angle increased from $0°$ to $90°$, the birefringence decreased from 0.003 to 0. The change was more gradual with OP angles near $0°$ and $90°$. The OP-dependent birefringence computed using both forms did not show a noticeable difference. In fact, they agreed with each other very well over the entire range of OOP angles.

Figure 2B shows the mean and SD of calculated OP angles based on 200 estimated δ_0' values at each OP angle. Overall, mean OP angles had a very good agreement with reference values, with discrepancy slightly larger at small OP angles. The largest mean difference of $6.1°$ was observed when all fibers were perfectly IP, an idealized condition unlikely to occur in actual tissues. The SD shows that the quantification of small OP angles was more sensitive to the retardance approximation errors while such quantification had a better tolerance on retardance approximation for large OP angles. The SD was less than $3.5°$ for OP angles larger than $25°$.

3.2 | Verification with chicken tendons

The chicken tendon imaging verified that OP fiber orientation can be accurately quantified with 3dPLM. Figure 3 shows the images of tendon at 7 OP angles, as well as the quantitative comparison between the measured and reference OP angles (the angles at which the tendon samples were set relative to the sectioning plane). The color images show the computed OP fiber orientations. A clear trend from cool colors to warm colors is observed as OP angles increase from $0°$ to $90°$. Tendons have roughly "tubular" shape, so the longitudinal section at $0°$ shows a larger sample of tissue with rectangular cross section, whereas the transverse section shows a shape closer to an ellipse, with oblique sections showing something in-between. The plot demonstrates that mean OP angles had a very good agreement with the reference OP angles. The SD exhibits similar characteristics as predicted in the analysis in Section 3.1. We observed smaller variations for large OP angles than that for small OP angles. It is important to consider that OP angle dispersion in tissues is not only due to the retardance approximation, but also due to actual intrinsic variations in the orientation of the fibers [22], as well as "noise" from non-collagenous tissues.

3.3 | 3dPLM imaging of ocular tissues

The results in this section demonstrate the performance of the technique in tissue samples with complex fiber organizations and the need of 3D fiber orientation quantification. The locations of imaged regions, peripapillary sclera, anterior sclera and cornea, are indicated with blue, green and red box, respectively, in Figure 1.

Figure 4A shows the bright field (BF) image of a 25-µm-thick sagittal sheep section at ×4 magnification. The peripapillary sclera region exhibits complex fiber organization, with both long fiber bundles (red arrowhead) and "hole-like" fiber bundle fascicles (green arrowhead) across the entire PPS region. The IP fiber orientation map (Figure 4B) shows both the morphology and color-coded orientation of IP fibers. While the sclera is dense with collagen fibers, the IP orientation map indicates fiber bundles with small OP angles are a small fraction of all the bundles, matching visible long fiber bundles in the BF image. In the OP fiber orientation map (Figure 4C), many fiber bundle fascicles with large OP angles can be recognized between fiber bundles with small OP angles. Figure 4D shows a close-up of the region-of-interest (ROI) indicated with a black box in Figure 4C. Two OP fiber bundle fascicles can be easily identified with IP fiber bundles between them. The fiber organization is perhaps better visualized by rendering the fibers in 3D as cylinders, as shown in Figure 4E.

The BF image of the anterior sclera (Figure 5A) shows fiber organizations. Across the section, long fiber bundles can be identified, which may suggest these fiber bundles
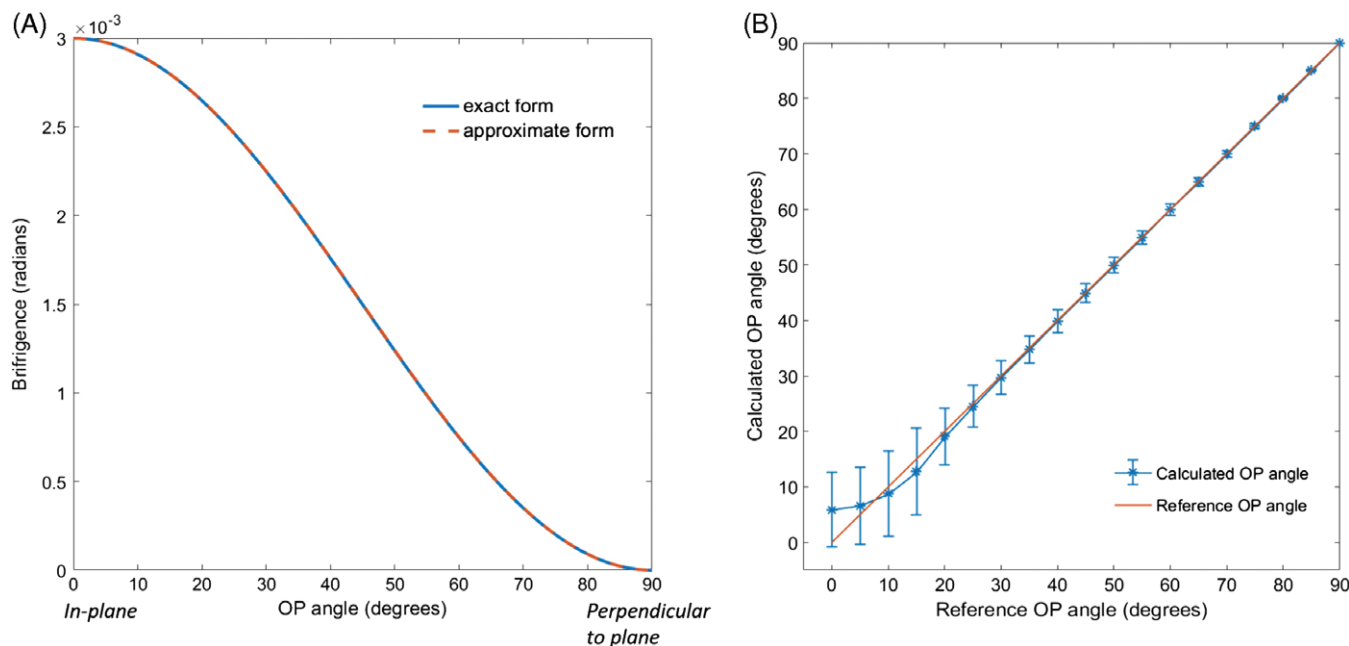
FIGURE 2 (A) Birefringence computed using both exact and approximate forms. (B) Calculated mean and dispersion (SD) of OP angles with the presence of retardance approximation error. The plot demonstrates that mean calculated OP angles agree very well with reference OP angles. The dispersion of the calculated values was slightly larger for small OP angles than for larger ones. The error bar represents SD

have small OP angles. In the inner sclera region, however, fiber bundles are shorter and wider than that in outer sclera region. In the IP fiber orientation map, the outer sclera shows a consistent fiber orientation of roughly 60° and the inner sclera shows a less uniform fiber orientation (Figure 5B). In a close-up of a small ROI indicated by a

FIGURE 3 OP fiber orientation mapping on 7 chicken tendon sections cryosectioned at known orientations from longitudinal (0°) to transverse (90°). Inset shows the photos of tendons as set at various orientations (top) as well as images colored by the local OP. The line plot shows a quantitative comparison. Calculated mean OP fiber orientation matched reference fiber orientations. The error bar represents the SD

white box, 2 collagen fiber populations can be identified with IP fiber orientation approximately perpendicular to each other. The fibers color coded in purple appear somewhat dim because of their low energy values, computed as described in the methods. Without additional information, IP fiber orientation could lead to an erroneous conclusion that these 2 fiber bundles run into each other. The OP fiber orientation map (Figure 5C), however, resolves this conflict, by revealing that the collagen fibers in the outer sclera are more IP (small OP angles) whereas those of the inner sclera have large OP and are therefore mainly perpendicular to the section. By synthesizing both IP (Figure 5B) and OP (Figure 5C) fiber orientation information, it is clear that collagen fibers in the outer sclera are mainly organized IP with an IP orientation of roughly 60°, and fibers in the inner sclera are running OP at approximately 75° while its projected IP fiber orientation is around 135°. Such fiber organization cannot be adequately described by neither fiber orientation maps alone. In a small ROI indicated with a dashed line black box, a 3D fiber orientation map was generated to better visualize 3D fiber organizations (Figure 5D). Figure 5E shows the cylinder-based 3D fiber rendering of a small ROI indicated with a white box in Figure 5D.
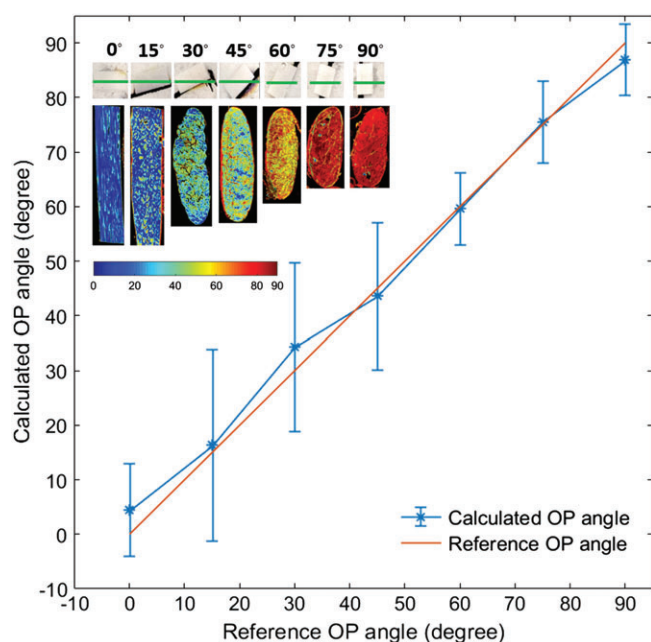
The cornea is known for its orthogonally organized lamellae structures [2]. This organization is essential to its optical transparency, refractive power and mechanical strength. The BF image (Figure 6A) shows clear fiber lamellae, with holes in-between that result from the tissue processing. The IP fiber orientation map shown in Figure 6B suggests that all fibers are oriented around 135° without revealing any information about the 3D perpendicular
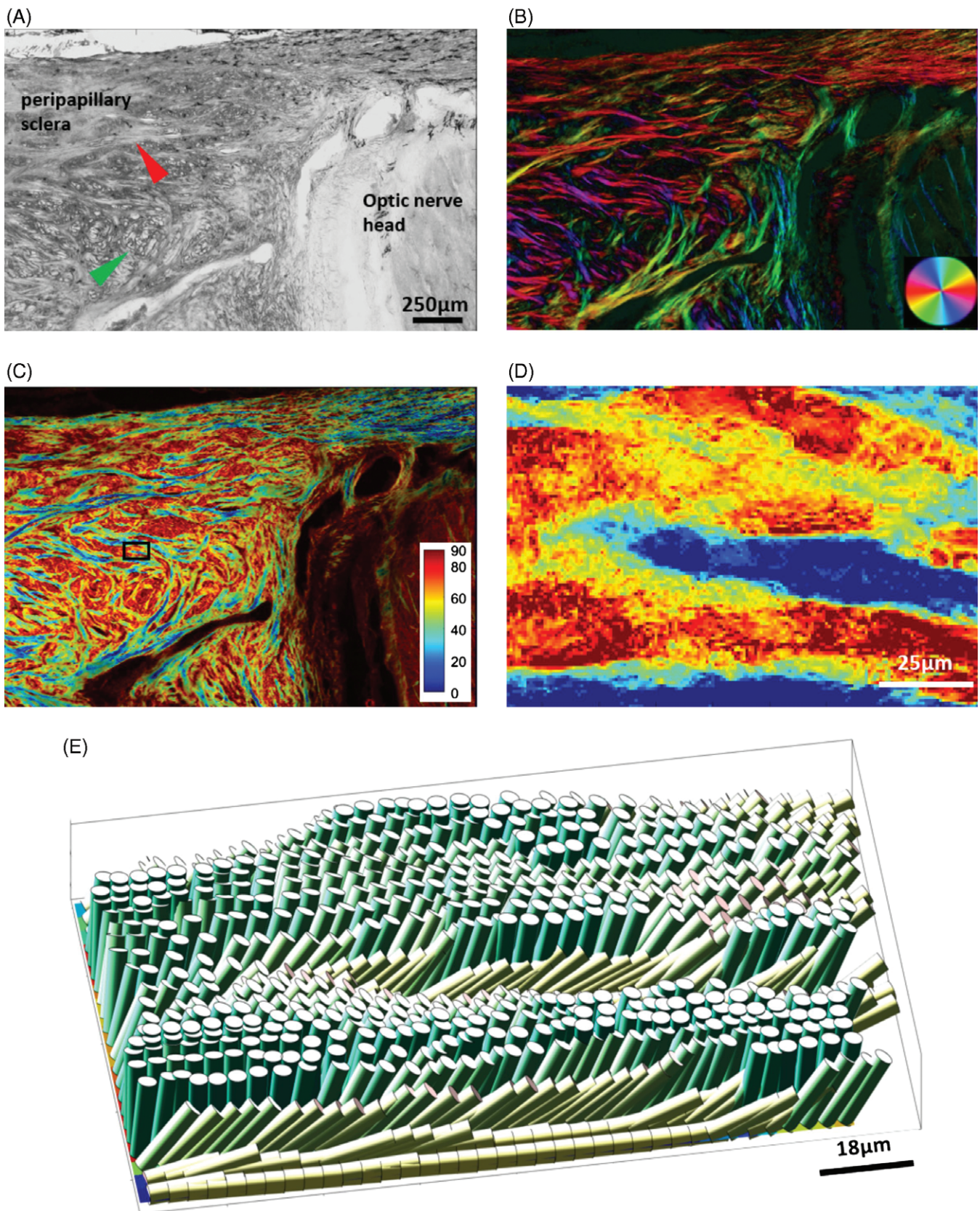
FIGURE 4 Application of 3dPLM to posterior pole of a sheep eye. (A) BF image with red and orange arrowheads pointing to long IP fiber bundles and OP fiber bundle fascicles, respectively. (B) IP fiber orientation map showing both IP fiber morphology and orientation. (C) OP fiber orientation map highlighting fiber bundle fascicles. (D) OP fiber orientation of small ROI shown in (C). (E) 3D visualization of collagen fibers
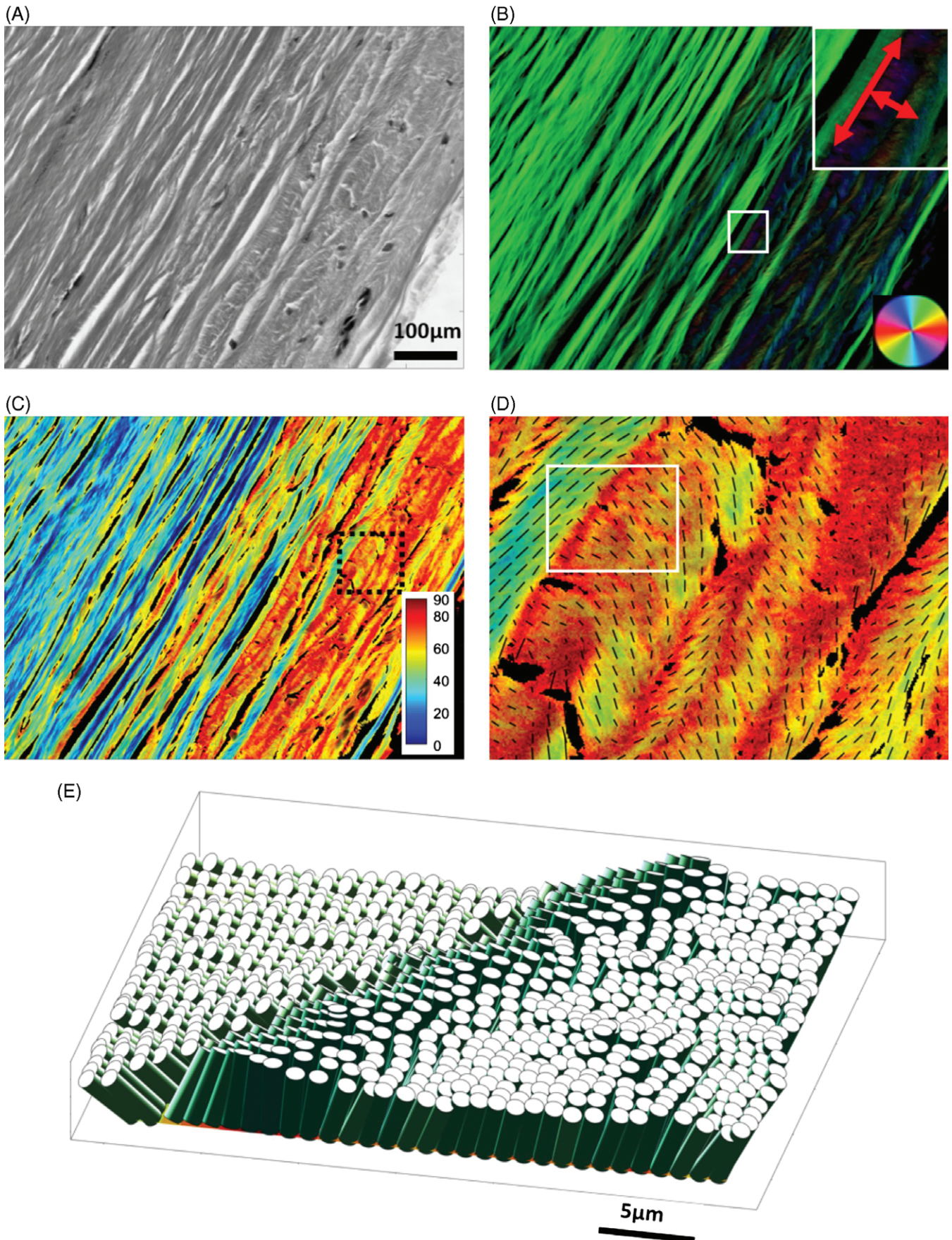
FIGURE 5 IP and OP fiber orientation map of the anterior sclera. (A) BF image of the sclera. The red box indicates the approximate location of the imaged region. (B) IP fiber orientation map of the sclera. Inset indicates the 2 perpendicular IP fiber orientation. (C) OP fiber orientation map of the sclera. (D) 3D fiber reconstruction on a small ROI indicated with a black box in (C). The orientation of the black lines represents the projected IP fiber orientation whereas the length of the line represents how OP the fiber is (large OP angles are shown by short lines and small OP angles by long lines). (E) 3D visualization of collagen fibers of an ROI indicated with a white box in (D)
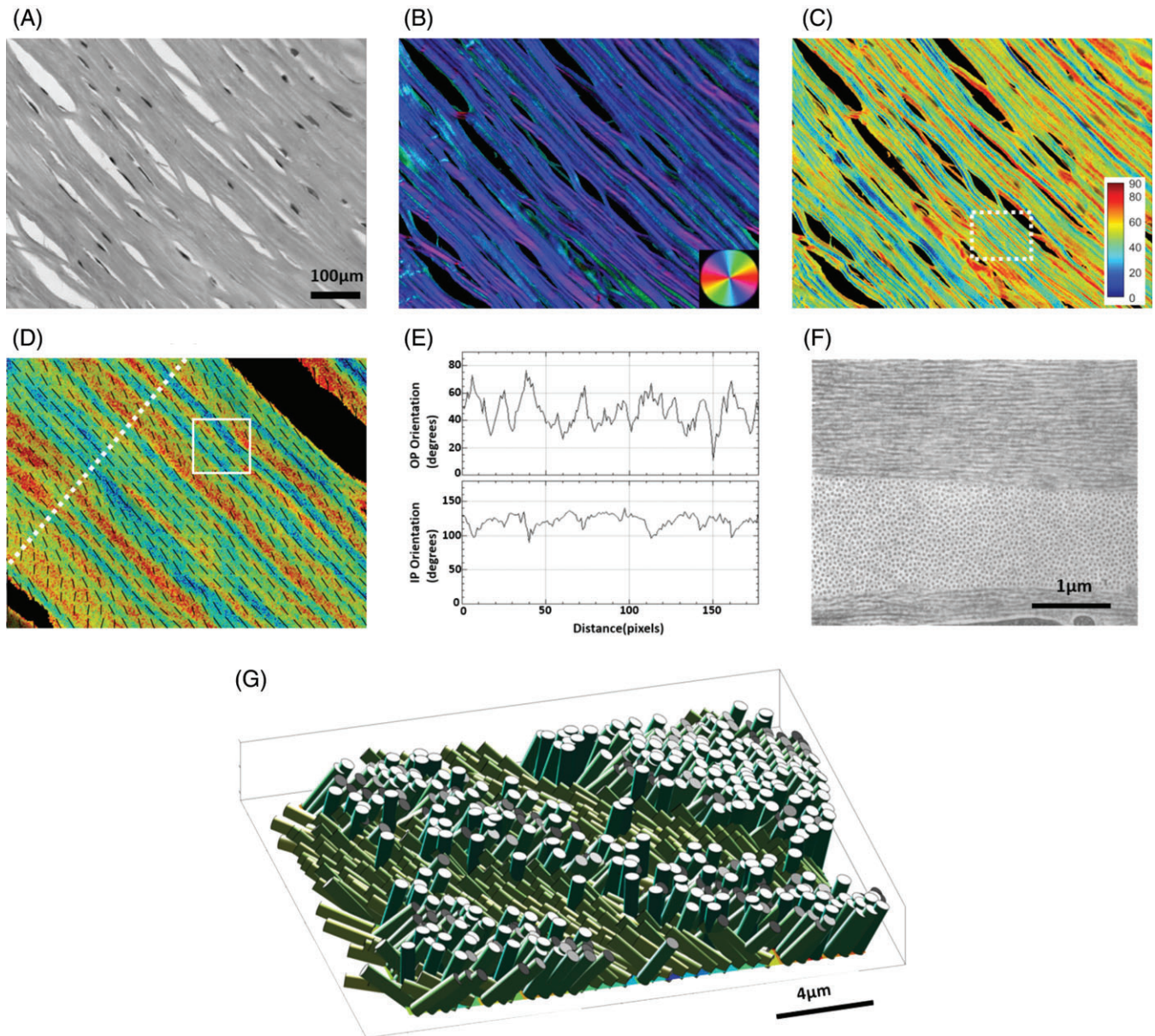
FIGURE 6 IP and OP fiber orientation map of the cornea. (A) BF image of the cornea. The red box indicates the approximate location of the imaged region. (B) IP fiber orientation map of the cornea. (C) OP fiber orientation map of the cornea. (D) 3D fiber orientation on a small ROI indicated with a white box in (C). The direction of the line indicates the fiber orientation, and the length of the line indicates inclination. (E) The IP and OP fiber orientation along a line ROI. (F) Electronic micrograph showing collagen fiber organization in cornea adapted from[28]. (G) 3D visualization of collagen fibers of an ROI indicated with a white box in (D)

lamellae organization. In the OP maps (Figure 6C), such structures are unambiguously visible with alternating low-/high OP fiber orientation. Note that, in this study, OP fiber orientation angles were measured between $0°$ and $90°$, without distinguishing an OP angle from its complementary one. Thus, the relative orientations of adjacent lamellae in Figure 6 are either $30°$ or $90°$, consistent with observations of $90°$ obtained using transmission electron microscopy (Figure 6F, adapted from [28]).

The 3D fiber orientation map of Figure 6D shows a small ROI in Figure 6C. A line profile was analyzed for IP and OP angles, shown in Figure 6E. By tracking a few successive peaks and valleys of OP angles, average peaks were centered approximately at $60°$ while valleys were at $30°$, which suggests that successive lamellae layers are orientated $90°$ to one another. The 3D cylinder-based fiber visualization of an ROI indicated with a white box in Figure 6D is shown in Figure 6G. This is an important confirmation of the ability to use quantitative 3dPLM orientation information to infer the 3D structure of ocular tissues.

4 | DISCUSSION

Understanding the complex 3D organization of collagen fibers in the eye requires a technique that can quantify the

collagen fiber orientation in 3D. In this manuscript, we have described 3dPLM, a method that allows quantification of both IP and OP fiber orientation in ocular tissues. We demonstrated that this information can help avoid potential errors and misunderstandings arising from interpreting fiber organization solely from 2D data. The performance of our imaging technique was validated on tendons, with results demonstrating good agreement between measured and known orientation. We imaged and quantified 3D fiber orientation on multiple regions of the eye, demonstrating the technique as a powerful tool to study the microstructure and architecture of ocular tissues.

Ocular shape is one of the primary determinants of ocular function. The 3D collagen microstructure and architecture are essential for maintaining this shape when acted upon by both intraocular and extraocular forces. For example, sharp vision relies on the refractive power of the cornea in the anterior pole of the eye, which, in turn, is highly sensitive to the radii of curvature of both the exterior and interior surfaces of the cornea. Even small changes in the cornea microstructure can have substantial effects on vision [1]. The ability to quantify the 3D microstructure of the cornea is therefore essential to understanding corneal physiology and pathophysiology, and to improving refractive surgical techniques. In the posterior pole, the 3D microstructure of the sclera is also critical in determining how force is transferred from the extraocular muscles and the optic nerve sheath to the corneoscleral shell [29]. The ability to quantitatively characterize the integration of these extraocular fibers into the scleral shell, in 3D, will be essential for understanding the biomechanical effects on the eye of changes in intracranial fluid pressure and gaze [30, 31].

In addition to enabling direct quantification of both IP and OP fiber orientations, 3dPLM has several key advantages over techniques typically used to characterize collagen fiber orientation in the eye, such as SALS[10], WAXS[7, 11] and multiphoton microscopy[15, 16]. 3dPLM is relatively simple, without requiring the complex and expensive systems needed for MPM or, especially, WAXS. 3dPLM is full-field (ie, non-scanning) and it is therefore fast, providing simultaneously high resolution and wide field of view. In addition, the conventional imaging techniques suffer multiple limitations when imaging ocular tissues. SALS and WAXS are suitable for thick tissue imaging. In thick tissues, however, the restriction to IP orientation is even more limiting. The scanning beamwidth, typically 100 to 300 μm in diameter, makes the resolution too low to resolve individual fiber bundles. The optical sectioning of multiphoton microscopy allows for the visualization of 3D collagen microstructures. Deriving 3D fiber orientation from 3D microstructures is not trivial and can be quite time-consuming.[15] In dense tissues, such as the sclera, it is difficult to achieve good penetration with a sufficient depth resolution for good 3D reconstructions. Thus, studies of ocular tissue typically quantify

only IP fiber orientation applying gradient-based techniques, such as local Fourier transform.[7] By requiring excellent fiber visibility, these analysis methods both increase the resolution and contrast demands, and increase the susceptibility to artifacts due to variations in signal. These variations can be, for example, due to the presence of pigment, which is common in the posterior pole of the eye. Compared to these traditional techniques, 3dPLM has a lower computational cost; when paired with an advanced camera[32] or multichannel imaging system[33], 3dPLM is well suited for time sensitive applications with the potential for real-time 3D fiber quantification.

As we have demonstrated, full 3D information is necessary for accurate characterization of the fiber organization. Conventionally, it is only possible to quantify IP fiber orientation in a specific plane, and the eye is, accordingly, sectioned longitudinally or coronally. Stacking data from 2D sections can be used to produce pseudo-3D information, occasionally enhanced by repeating the process in another sample analyzed in a perpendicular direction. The results, however, are susceptible to artifacts, for example, due to sample variability, and are much more complex and time-consuming to obtain. Most importantly, they will have low sensitivity to characterize small or uncommon features. 3dPLM, in contrast, can extract both IP and OP fiber orientation from the same section. IP and OP fiber orientation maps can then be used to infer 3D fiber microstructure, with the stacking used to extend these to a volume. Since traditional techniques produce 2D data, biomechanical modeling of the eye has also traditionally employed fiber distributions in the plane (transversely isotropic or anisotropic). These may be sufficient only for gross modeling of the ocular shell[30, 34], but when precise or microstructure aware models are needed, the assumptions from 2D data are likely not enough [5, 35]. In the past decade, the morphometry and analysis of the eye have moved from 2D to 3D which led to huge gains in the understanding of the eye.[36–38] In this same vein, the 3dPLM imaging technique we propose here will also enable a leap in understanding of the eye with the availability of 3D microstructure data.

Several assumptions were made to quantify OP fiber orientation. We assumed maximal tissue retardance did not vary much and the retardance from 1 region was extended across the entire imaged area. This method poses fewer restrictions on sample preparation and simplifies the analysis when compared with methods that require laborious calibration[19] or other data on tissue properties[39]. Calibration-based methods are particularly difficult for cryosectioned soft tissues as section thickness could vary slightly from 1 section to the other. Such issues had minimal effects on the OP angle quantification by 3dPLM as the maximal retardance was estimated from and later applied to the same sample. Moreover, the retardance incorporates the combined effects of tissue thickness and birefringence, and therefore the method

can be applied to tissue sections without explicit knowledge of the thickness and birefringence, which are essential for other techniques. Nevertheless, actual retardance could vary over a section, for example, if section thickness is not uniform. Future work could improve the accuracy of our technique by using, for example, fluorescent labeling for the collagen. This would require, however, a highly consistent label, which is not trivial, and would make the process slower and more complex. 3dPLM takes advantage of the strong effects of OP angle on the retardance. However, in addition to OP angle, retardance may also be affected by fiber dispersion. Our calculations of IP and OP angles were based on the assumption of low fiber dispersion. While this assumption seems reasonable for thin sections imaged with micron-scale resolution, it is important to be cautious when interpreting results in regions with high fiber dispersion to avoid misinterpreting findings. Also, some applications might require distinguishing between complementary OP angles. Future techniques could do this, by optical methods, or perhaps by integrating information from neighboring sections.

During tissue processing, an OCT compound was used as part of the cryosectioning procedure. This is necessary to protect the tissues from potential damaging effects of freezing by reducing ice crystal formation[40]. Although some chemical compounds may change optical properties[41, 42], we are confident that OCT did not affect the results presented for the following reasons: First, before imaging, the sections were rehydrated with PBS. OCT is water soluble, and it is therefore "washed" away. We have compared sections before and after through "washing" the OCT, and detected no changes. Second, OCT from Fisher HealthCare is not the only cryoprotecting compound available. In preliminary tests, we compared OCT with compounds from other brands, and detected no differences. Finally, the results in this work were derived from a ration computation (Eq. (9)). Hence, even if the signal was slightly affected by the presence of OCT, the effects would likely cancel out.

The goal of this work was to study 3D fiber orientation in thin sections. Thin sections are used routinely in a large number of studies, in part because they are suitable for immuno-histochemistry. Thus, the techniques we present can be readily added to ongoing studies. Future work would benefit from developing techniques that enable 3D fiber orientation in bulk tissues or thick sections. Thick tissues present important challenges, such as strong tissue scattering and imaging depth-of-field. Techniques for addressing these challenges are in development. For example, elsewhere we have demonstrated that using PLM with structured light illumination allows quantifying IP fiber orientation of thick tissues[43].

5 | CONCLUSION

We have demonstrated that 3dPLM is a robust and effective approach to quantify and visualize 3D fiber orientation in ocular tissues. The 3D fiber orientation, in turn, enables us to better study complex collagen fiber microstructures and improves our understanding of the role of ocular biomechanics in both health and disease. The 3dPLM technique is system independent and can potentially be added to existing microscopy systems to perform a comprehensive assessment of collagen fiber orientation and architecture on ocular tissues as well as other collagenous tissues.

Conflict of interest

None.

ORCID

Ian A Sigal http://orcid.org/0000-0002-0790-7911

REFERENCES

[1] M. Winkler, G. Shoa, Y. Xie, S. J. Petsche, P. M. Pinsky, T. Juhasz, D. J. Brown, J. V. Jester, *Invest. Ophthalmol. Vis. Sci.* **2013**, *54*, 7293.

[2] K. M. Meek, C. Knupp, *Prog. Retin. Eye Res.* **2015**, *49*, 1.

[3] T. J. Freegard, *Eye* **1997**, *11*, 465.

[4] R. Grytz, M. A. Fazio, M. J. Girard, V. Libertiaux, L. Bruno, S. Gardiner, C. A. Girkin, J. C. Downs, *J. Mech. Behav. Biomed. Mater.* **2014**, *29*, 602.

[5] A. Voorhees, N.-J. Jan, I. Sigal, *Acta Biomaterialia* **2017**, *58*, 278.

[6] J. A. S. Rada, S. Shelton, T. T. Norton, *Exp. Eye Res.* **2006**, *82*, 185.

[7] J. K. Pijanka, B. Coudrillier, K. Ziegler, T. Sorensen, K. M. Meek, T. D. Nguyen, H. A. Quigley, C. Boote, *Invest. Ophthalmol. Vis. Sci.* **2012**, *53*, 5258.

[8] G. Wollensak, E. Spoerl, T. Seiler, *Am. J. Ophthalmol.* **2003**, *135*, 620.

[9] R. Mercatelli, F. Ratto, F. Rossi, F. Tatini, L. Menabuoni, A. Malandrini, R. Nicoletti, R. Pini, F. S. Pavone, R. Cicchi, *J. Biophotonics* **2017**, *10*, 75.

[10] M. J. Girard, A. Dahlmann-Noor, S. Rayapureddi, J. A. Bechara, B. M. Bertin, H. Jones, J. Albon, P. T. Khaw, C. R. Ethier, *Invest. Ophthalmol. Vis. Sci.* **2011**, *52*, 9684.

[11] H. Aghamohammadzadeh, R. H. Newton, K. M. Meek, *Structure* **2004**, *12*, 249.

[12] N.-J. Jan, J. L. Grimm, H. Tran, K. L. Lathrop, G. Wollstein, R. A. Bilonick, H. Ishikawa, L. Kagemann, J. S. Schuman, I. A. Sigal, *Biomed. Opt. Express* **2015**, *6*, 4705.

[13] V. V. Tuchin, L. Wang, D. A. Zimnyakov, *Optical Polarization in Biomedical Applications*, Springer Science & Business Media, New York, **2006**.

[14] V. V. Tuchin, *J. Biomed. Opt.* **2016**, *21*, 071114.

[15] X. Chen, O. Nadiarynkh, S. Plotnikov, P. J. Campagnola, *Nat. Protoc.* **2012**, *7*, 654.

[16] M. Han, G. Giese, J. F. Bille, *Opt. Express* **2005**, *13*, 5791.

[17] S. Psilodimitrakopoulos, I. Amat-Roldan, P. Loza-Alvarez, D. Artigas, *Biomed. Opt. Express* **2012**, *3*, 2681.

[18] M. Born, E. Wolf, *Principles of Optics: Electromagnetic Theory of Propagation, Interference and Diffraction of Light*, Elsevier, New York **2013**.

[19] E. M. Spiesz, W. Kaminsky, P. K. Zysset, *J. Struct. Biol.* **2011**, *176*, 302.

[20] A. N. Bashkatov, E. A. Genina, V. I. Kochubey, V. V. Tuchin, Estimation of wavelength dependence of refractive index of collagen fibers of scleral tissue. in *Controlling Tissue Optical Properties: Applications in Clinical*

Study. SPIE Proceedings, Vol. 4162 (Ed: V. V. Tuchin), SPIE, Bellingham, WA **2000**, p. 265.

[21] J. F. De Boer, T. E. Milner, M. J. van Gemert, J. S. Nelson, *Opt. Lett.* **1997**, *22*, 934.

[22] P. Fratzl, *Collagen: Structure and Mechanics*, Springer, New York **2008**, p. 1.

[23] H. Tran, N.-J. Jan, D. Hu, A. Voorhees, J. S. Schuman, M. A. Smith, G. Wollstein, I. A. Sigal, *Sci. Rept.* **2017**, *7*, 12065.

[24] R. A. Farrell, R. L. McCally, *Principles Pract. Ophthalmol.* **2000**, *2*, 629.

[25] D. Freund, R. McCally, R. Farrell, *JOSA A* **1986**, *3*, 1970.

[26] R. Farrell, D. Freund, R. McCally, MRS Online Proc. Library Arch. **1991**, 255.

[27] R. A. Farrell, D. E. Freund, R. L. McCally, *Johns Hopkins Appl. Physics Lab. Techn. Digest.* **1990**, *11*, 2.

[28] Y. Komai, T. Ushiki, *Invest. Ophthalmol. Vis. Sci.* **1991**, *32*, 2244.

[29] Y. Hua, A. P. Voorhees, I. A. Sigal, *Invest. Ophthalmol Vis. Sci.* **2018**, *59*, 154.

[30] X. Wang, M. R. Beotra, T. A. Tun, M. Baskaran, S. Perera, T. Aung, N. G. Strouthidis, D. Milea, M. J. Girard, *Invest. Ophthalmol. Vis. Sci.* **2016**, *57*, 5825.

[31] B. Wang, H. Tran, M. A. Smith, T. Kostanyan, S. E. Schmitt, R. A. Bilonick, N.-J. Jan, L. Kagemann, E. C. Tyler-Kabara, H. Ishikawa, J. S. Schuman, I. A. Sigal, G. Wollstein, *PLOS ONE* **2017**, *12*, e0188302.

[32] V. Gruev, R. Perkins, T. York, *Opt. Express* **2010**, *18*, 19087.

[33] W. Kaminsky, E. Gunn, R. Sours, B. Kahr, *J. Microsc.* **2007**, *228*, 153.

[34] M. D. Roberts, I. A. Sigal, Y. Liang, C. F. Burgoyne, J. C. Downs, *Invest. Ophthalmol. Vis. Sci.* **2010**, *51*, 5675.

[35] H. Yi, A. P. Voorhees, I. A. Sigal, *Invest. Ophthalmol. Vis. Sci.* **2017**.

[36] I. A. Sigal, J. G. Flanagan, I. Tertinegg, C. R. Ethier, *Exp. Eye Res.* **2010**, *90*, 70.

[37] H. Yang, H. Thompson, M. D. Roberts, I. A. Sigal, J. C. Downs, C. F. Burgoyne, *Invest. Ophthalmol. Vis. Sci.* **2011**, *52*, 345.

[38] N. G. Strouthidis, B. Fortune, H. Yang, I. A. Sigal, C. F. Burgoyne, *Invest. Ophthalmol. Vis. Sci.* **2011**, *52*, 1206.

[39] M. Menzel, K. Michielsen, H. De Raedt, J. Reckfort, K. Amunts, M. Axer, *J. Royal Soc. Interface* **2015**, *12*, 20150734.

[40] A. H. Fischer, K. A. Jacobson, J. Rose, R. Zeller, *Cold Spring Harb. Protoc.* **2008**, *3*(8), 1.

[41] A. T. Yeh, B. Choi, J. S. Nelson, B. J. Tromberg, *J. Invest. Dermatol.* **2003**, *121*, 1332.

[42] E. A. Genina, A. N. Bashkatov, Y. P. Sinichkin, V. V. Tuchin, *Quantum Elec.* **2006**, *36*, 1119.

[43] B. Yang, B. Brazile, N.-J. Jan, A. P. Voorhees, I. A. Sigal, *Structured Polarized Light Microscopy (SPLM) for Mapping Collagen Fiber Orientation of Ocular Tissues*, Vol. 10546, International Society for Optics and Photonics, Bellingham, WA **2018**, p. 105460I.